JCTC Journal of Chemical Theory and Computation

Article

pubs.acs.org/JCTC

Constant-pH MD Simulations of DMPA/DMPC Lipid Bilayers

Hugo A. F. Santos,[†] Diogo Vila-Viçosa,[‡] Vitor H. Teixeira,[‡] António M. Baptista,[¶] and Miguel Machuqueiro*[,‡]

[†]BioISI—Biosystems & Integrative Sciences Institute, Faculdade de Ciências and [‡]Centro de Química e Bioquímica and Departamento de Química e Bioquímica, Faculdade de Ciências, Universidade de Lisboa, 1749-016 Lisboa, Portugal

[¶]Instituto de Tecnologia Química e Biológica António Xavier, Universidade Nova de Lisboa, Av. da República, 2780-157 Oeiras, Portugal

Supporting Information

ABSTRACT: Current constant-pH molecular dynamics (CpHMD) simulations provide a proper treatment of pH effects on the structure and dynamics of soluble biomolecules like peptides and proteins. However, addressing such effects on lipid membrane assemblies has remained problematic until now, despite the important role played by lipid ionization at physiological pH in a plethora of biological processes. Modeling (de)protonation events in these systems requires a proper consideration of the physicochemical features of the membrane environment, including a sound treatment of solution ions. Here, we apply our recent CpHMD-L method to the study of pH effects on a 25% DMPA/DMPC bilayer membrane model, closely reproducing the correct lipid phases of this system, namely, gel—fluid coexistence at pH 4 and a fluid phase at pH 7. A significant transition is observed for the membrane ionization and mechanical properties at physiological pH, providing a molecular basis for the well-established role of phosphatidic acid (PA) as a key player in the regulation of many cellular events. Also, as reported experimentally, we observed pH-induced PA—PA lipid aggregation at acidic pH. By including the titration of anionic phospholipids, the current methodology makes possible to simulate lipid bilayers with increased realism. To the best of our knowledge, this is the first simulation study dealing with a continuous phospholipid bilayer with pH titration of all constituent lipids.

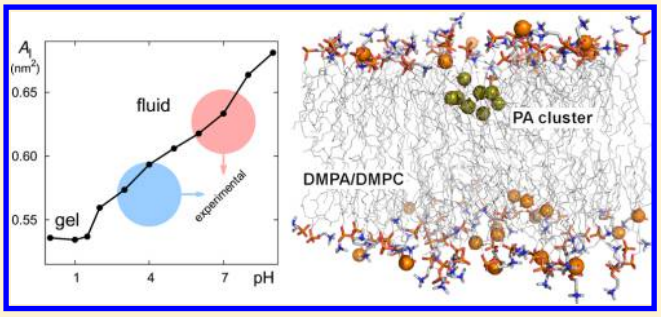

1. INTRODUCTION

Despite being exceptionally small and one of the most simple chemical species, protons play a central role in the life of cells. Many physicochemical reactions in living cells involve exchange of these hydrogen ions, and changes in its concentration are intimately tied to the charge presented not only by amino acid side chains in proteins but also by the titrable head groups of some ionizable lipids.[1,2] The induction of reversible chemical changes through ionization events results in substantial electrostatic perturbation, ultimately affecting the interaction of the titrable macromolecule with the surrounding environment in a structural, dynamical, and functional way.[1,3−5]

Even though cytosolic pH homeostasis is tightly regulated, it fluctuates, on average, one pH unit within the physiological range.[1,3] Both proteins and lipids are sensitive to such fluctuations—for the former, this dependence is well established being that pH is one of the main regulators of the activity of several key enzymes and metabolic pathways.[1,3,4] As for lipids, the role of pH is often disregarded, given that most biophysical models are based on pure zwitterionic lipids, which do not titrate. Although pH has limited impact on such lipids, the same does not apply when dealing with mixtures with an even small content of anionic lipids titrating in the physiological range. In fact, a large number of biological membranes have anionic lipids in their constitution, which render them pH-sensitive.[6,7]

Irrespective of its structural simplicity, phosphatidic acid (PA) occupies a key position in many metabolism and biogenesis related processes in all domains of life.[8] Recent studies using yeast as a model organism, established PA as a pH biosensor.[6,9] Under nutrient depletion conditions (acidic pH), the negative transcriptional regulator Opi1 is released from the ER membrane to the cytosol to inhibit membrane biogenesis. A rapid and significant decrease in intracellular pH results in increased protonation of its phosphomonoester, thereby reducing the strength of the electrostatic interactions with its effectors.[10] Thereby, pH-modulated PA binding of Opi1 is the mechanistic basis of the coupling between membrane biogenesis and general metabolism.[9] This anionic lipid has a complex pH titration behavior where it can exchange one or two protons, exhibiting different mixtures of charges (0, −1, and −2) at physiological pH.[11,12] Experiencing two (de)protonation reactions, one of which is expected to be in the physiological pH range, PA has been proposed to vary significantly its charge

Received: October 7, 2015
Published: November 12, 2015

DOI: 10.1021/acs.jctc.5b00956
J. Chem. Theory Comput. 2015, 11, 5973−5979

according to small changes in solution pH and therefore to bind proteins in a pH-dependent manner.[7]

We have been extending the stochastic constant-pH MD method[13−25] to deal with lipid bilayers, where the lipids are allowed to change their protonation states.[25] This new CpHMD-L method requires a correct description of the periodic boundary conditions in the Poisson−Boltzmann (PB) calculations[26] and a methodology to correctly treat the ionic strength effect close to charged lipid bilayers.[12] These charged bilayers induce, in the simulation boxes, local counterion concentrations significantly higher than bulk ionic strength but not enough to achieve the system's neutrality.[12,25,27−35] In a previous work, we have devised and tested a new PB-based method to estimate the number of ions near to a 25% DMPA/DMPC lipid bilayer.[12] Using MD simulations and PB calculations, we showed that our approach is correctly modeling the ionization dependent isothermal phase transition of the bilayer observed experimentally.[36]

In this work, we extend our CpHMD-L method to simulate the pH effects on the DMPA/DMPC phospholipid mixture in a bilayer environment. A complete titration profile of this system will provide valuable information on the ionization degree of the bilayer close to physiological pH. As far as we know, this study constitutes the first CpHMD approach where all phospholipids are allowed to titrate, bringing a new level of realism to MD simulations of such biophysical systems.

2. METHODS

2.1. CpHMD-L Settings and System Setup. CpHMD-L is an extension of the stochastic titration method,[13,14] consisting of three successive steps that are cyclically repeated during the simulations: (1) PB/MC to sample the protonation states, (2) MM/MD during a time τ_{rlx} to relax the solvent around a frozen solute, and (3) unrestrained MM/MD during a time τ_{prt}. In our previous work, we showed that τ_{rlx} = 0.2 ps and τ_{prt} = 20 ps lead to structurally stable membrane simulations and to extensive sampling of the protonation states, which consequently leads to a smaller chance of falling into kinetic traps during the simulations.[25]

Our lipidic systems are composed of 128 lipid molecules, a varying number of water molecules and Na^+/Cl^- counterions. In a previous study, we have shown that changing the counterion from Na^+ to K^+ did not influence significantly the behavior of these systems.[12] We studied pure DMPC and a 25% DMPA/DMPC mixture (32 PA and 96 PC molecules). The hydration of the bilayer depends on the average area per lipid (A_l) to ensure the existence of a small bulk-like water region not seen by any lipid. This region is kept relatively small avoiding significant trapping of ions.[12,25] The numbers of co- and counterions used depend on the ionization of the system at the ionic strength of 0.1 M and were estimated using a PB-based formalism previously described.[12,25] Several systems with different ionization values and estimated number of ions were equilibrated using MM/MD (see Tables S1 and S2 in the Supporting Information) and used as initial guesses for the CpHMD-L simulations. The 100% DMPC system was simulated at pH values of 0.0, 1.0, and 2.0 (Table S1). The 25% DMPA/DMPC system was simulated at pH values between 0.0 and 9.0, with 1 unit steps (Table S2). In this system, we did an extra simulation at pH 1.5 in order to improve our sampling of this region. Relatively long equilibration periods (20−50 ns) were done in our CpHMD-L simulations, followed by 70−90 ns of production runs (see Table S3).

2.2. Molecular Dynamics Settings. All MD simulations were performed using the GROMOS 54A7 force field[37] in a modified version of the GROMACS distribution (version 4.0.7)[13,14] and with the SPC water model.[38] The atomic partial charges of the lipid molecules were the ones previously published.[12,26]

The simulations were done in the NPT ensemble, using the v-rescale thermostat[39] at 310 K with separate couplings for the "solute" (lipids) and solvent (water and ions) with a relaxation time of 0.1 ps. The gel−liquid crystal phase transition temperature of DMPC is ∼297 K, and since DMPC is the major lipid constituent of our membrane systems, an absolute temperature of 310 K assures that the lipid bilayer is mostly in the liquid-crystalline phase state. On the other hand, the correspondent transition temperature for DMPA is very dependent on the solution pH.[36,40] A semi-isotropic Berendsen[41] pressure couple was used to maintain the pressure constant at 1 bar with a compressibility of 4.5×10^{-5} bar^{-1} and a relaxation time of 5.0 ps. The bond lengths of all molecules were constraint using the Parallel Linear Constraint Solver (P-LINCS) algorithm.[42] An integration step of 2 fs was used for the equations of motion in all MD simulations.

Nonbonded interactions were treated with a twin-range cutoff, with short- and long-range cutoffs of 8 and 14 Å, respectively. The neighbor pair list was updated every 5 steps. Long-range electrostatics interactions were treated using the generalized-reaction-field method,[43] with a relative dielectric constant of 54.0[44] and ionic strength of 0.1 M, being treated as an external parameter.[14]

The energy minimization procedure consisted of 10 000 steps using the steepest descent algorithm (unconstrained) followed by another 10 000 steps using the low-memory Broyden−Fletcher−Goldfarb−Shanno (*l-bfgs*) integrator (unconstrained) and yet another 100 steps using again the steepest descent algorithm (with all bonds constrained). The initiation of all systems consisted of a 50 ps simulation with all heavy atoms harmonically restrained to their respective fixed reference positions with a force constant of 1000 $kJ{\cdot}nm^{-2}{\cdot}mol^{-1}$. This first initiation step was followed by three other steps of 100, 150, and 200 ps simulations, respectively. Throughout these last three steps, the positions restraints were applied differently to phosphorus atoms and all the other heavy atoms. Hence, the force constants were 1000, 100, and 10 $kJ{\cdot}nm^{-2}{\cdot}mol^{-1}$ for the phosphorus atoms pertaining to the phosphate headgroups of all lipids, whereas all other heavy atoms motion potentials were restrained with force constants of 100, 10, and 0 $kJ{\cdot}nm^{-2}{\cdot}mol^{-1}$.

The MD simulations of all bilayer systems were pre-equilibrated for 100 ns, at which point three replicates were started for 100 ns equilibration runs. The first 20 ns were disregarded, and the last 80 ns were used to assess equilibration. These equilibrated systems presented a wide variety of ions and were used to initiate our CpHMD-L simulations. An *a priori* estimation of the ionization at a given pH value was needed to choose the correct system.

2.3. PB/MC Settings for CpHMD-L Simulations. The PB calculations were done with the program DelPhi V5.0[45,46] using atomic radii derived from GROMOS 54a7 force field[47] and atomic partial charges from previous works.[12,26] The molecular surface of the membrane was defined by a probe of radius 0.14 nm, and the ion exclusion layer was 0.2 nm. In order to avoid discontinuities of the molecular surface at the box boundaries, we added a small portion (5% of the box side dimension) of the membrane atoms in the *x* and *y* directions.[26] Periodic boundary

DOI: 10.1021/acs.jctc.5b00956
J. Chem. Theory Comput. 2015, 11, 5973−5979

conditions were explicitly applied along those two directions in the calculation of the potential. A convergence threshold value based on maximum change of potential of 0.01 k_BT/e was used. All PB calculations were done using cubic grids with 61^3 grid points and a two-step focusing procedure[48] with successive grid spacing of ∼0.1 nm and ∼0.025 nm. In the iteration convergence process of the finite differences method, we used relaxation parameters for the nonlinear and linear forms of the PB equation with values of respectively 0.75 and 0.20. A cutoff of 2.5 nm was used to calculate the background and pairwise interactions (see ref 26 for more details). The pK_a values of the model compounds used were 1.29 for DMPC (the pK_a value of dimethylphosphate) and 1.54 and 6.31 for DMPA (the two pK_a values of methylphosphate).[49] The dielectric constant of the solvent was 80, and for the membrane we used a value of 2.

The MC sampling was performed with the PETIT program[50] version 1.6.1 using an absolute temperature of 310 K. All runs were performed using 10^5 MC cycles, where one cycle consists of sequential state changes over all individual sites and pairs of sites with an interaction larger than 2 pH units.

2.4. PB Settings for Ion Estimation. The PB calculations performed for the ion estimation were similar to those described in a previous section. The focusing procedure was not used since we were interested in all grid points closer than 1.4 nm to the membrane. In the iteration convergence process of the finite differences method, we used relaxation parameters for the nonlinear and linear forms of the PB equation with values of respectively 0.15 and 0.20. In these calculations, we used 200 configurations from each simulation. To estimate the number of ions, the electrostatic potential was written to a new 3D grid with 50 points per side, the same size as the finite differences grid.[26] The number of cations, Na^+, and of anions, Cl^- (see Tables S2 and S3 in the Supporting Information), were calculated according to the previously published procedure.[12,25]

2.5. Analyses. The equilibrated portions of each simulation were used for analyses. A_l and deuterium order parameters were obtained using several tools from the GROMACS software package.[51,52] Membrane thickness and DMPA clustering were calculated using in-house tools. Membrane thickness was defined as twice the average z distance between each phosphorus atom and the center of mass (also in z) of all phosphorus atoms. All presented errors were computed using standard methods based on the autocorrelation function of the property measured to determine the number of independent blocks in the simulations.[53]

3. RESULTS AND DISCUSSION

3.1. pH Titration. From our CpHMD-L simulations, we are able to perform complete pH titration experiments. The titration curves were computed by averaging at each pH value the occupancy states of all titrable sites over the final equilibrated segments. Figure 1a shows how the total membrane charge fluctuates at different pH values. These well-behaved curves confirm that the simulation systems are equilibrated. Figure 1b presents a total pH titration curve and the two separate contributions from DMPA and DMPC. It is clear that, at pH > 4, PC is completely deprotonated, and only PA is sensitive to pH. Between pH 6 and 8 the titration curve seems to become slightly more abrupt, corresponding to the transition from PA^{-1} to PA^{-2}. Remarkably, our CpHMD-L method is able to correlate this abruptness with large fluctuations in the membrane charge (see pH = 7 of Figure 1a), a phenomenon already observed in an oleic acid bilayer,[25] which is an important

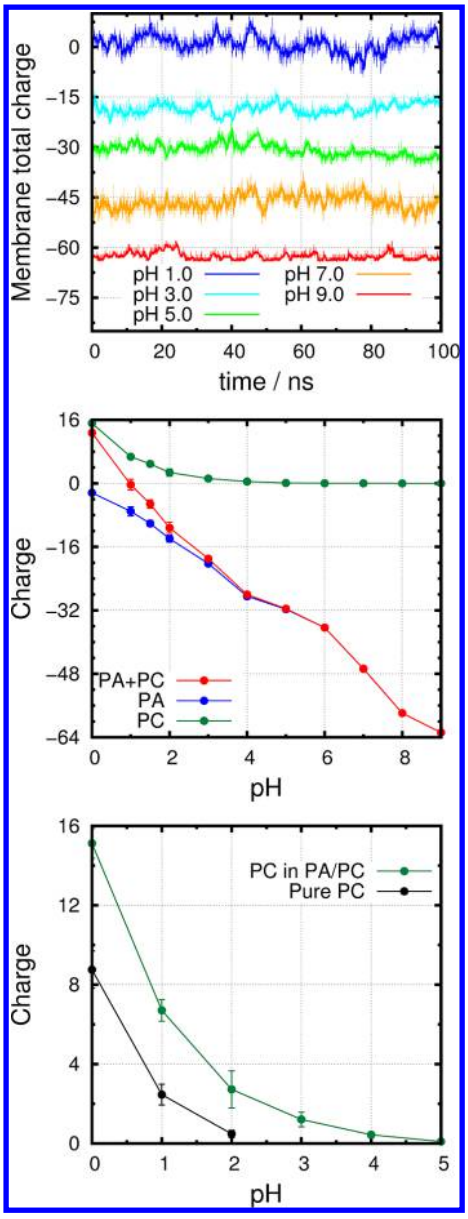

Figure 1. pH titration of the 25% DMPA/DMPC lipid bilayer. Membrane charge versus simulation time for one representative replicate per pH (**A**). Simulated titration curves for the whole system and the individual contributions from PA and PC (**B**). Comparison between the PC titration curves obtained from pure DMPC and from the 25% DMPA/DMPC mixture (**C**).

test of thermodynamic consistency for the sampling of protonation states (see Figure S1 in the Supporting Information). At more acidic pH values there is a significant contribution from DMPC to the overall total charge, resulting in positive values at pH < 1.0. In our previous study, we estimated the ionization of the 25% DMPA/DMPC system at pH 4.0 and 7.0 using PB/MC calculations over conformational ensembles extracted from MD simulations.[12] At pH 7.0 we estimated the total charge to be ∼−44,[12] which is in excellent agreement with the CpHMD-L value (∼−46). However, at pH 4.0 the PB/MC estimated charge value (∼−18)[12] is significantly lower than the one observed in this work (∼−28), which could be explained by the difference in the quality of the conformational sampling used. Figure 1c compares the titration curves of DMPC in pure lipid or 25% DMPA/DMPC mixture bilayers. The titration

DOI: 10.1021/acs.jctc.5b00956
J. Chem. Theory Comput. 2015, 11, 5973−5979

curve of pure DMPC indicates that the protonation of the first lipid in an infinite bilayer of zwitterionic DMPC only appears at pH ∼ 2.0, which is in very good agreement with our previous estimation using a Linear Response Approximation method (∼2.2−2.6).[26] The presence of a number of negatively charged DMPA lipids induces a shift in the PC titration curve toward higher pH values (Figure 1c) due to the electrostatic repulsion between ionized phosphates, stabilizing the PC^{+1} species with a neutral phosphate group.

Figure 2 shows the relative abundancies of the three PA protonation states (PA^0, PA^{-1}, and PA^{-2}) over the studied pH

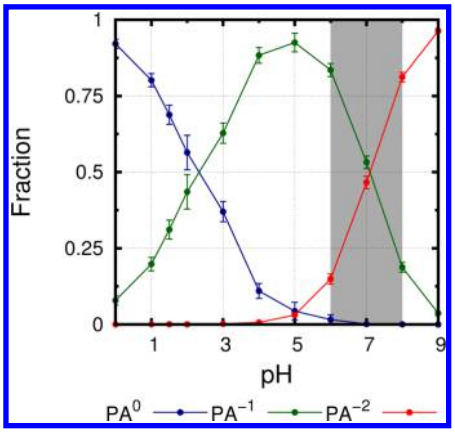

Figure 2. pH dependence of the fraction of the three predominant protonation states in DMPA. The physiological pH region was highlighted in gray.

range. From these results, we observe a coexistence region for the three charge states in the pH range of 4−6. Also, there are two main transition regions around pH 2.5 ($PA^0 \Rightarrow PA^{-1}$) and pH 7.0 ($PA^{-1} \Rightarrow PA^{-2}$), consistent with the total titration curve (Figure 1b). Interestingly, the transition at physiological pH (Figure 2) indicates that any slight changes in the solution pH will have a major impact on the charge densities of membranes containing significant amounts of this lipid. This implicates PA as a key player in the regulation of many cellular events, as suggested by several authors.[6,7,9,10]

3.2. Structural Properties of the DMPA/DMPC Lipid Bilayer. Figure 3 shows a pH-induced isothermal phase transition for the 25% DMPA/DMPC lipid bilayer. The A_l varies from ∼53 Å^2, at low pH values (almost in the typical gel phase region of DMPC), to ∼68 Å^2 at pH 9.0, which is well

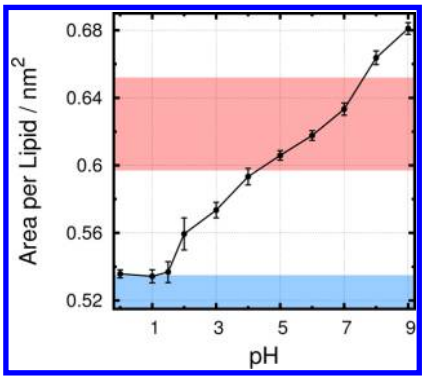

Figure 3. A_l variation with pH value for the 25% DMPA/DMPC lipid bilayer. Typical experimental values ranges for gel and liquid crystalline phases of DMPC are marked in blue and red, respectively.[54−63]

beyond the fluid phase region for DMPC. These results are in good agreement with our previously published data of A_l in several systems with different PA ionizations.[12] Nevertheless, at low pH values, we are not able to achieve A_l values as low as the ones reported for the zero charge PA system (∼49 Å^2) in that study.[12] This is probably because in the CpHMD-L simulations, DMPC was allowed to titrate, which at low pH values, originated several protonated DMPC molecules, slightly favoring larger A_l. Garidel and co-workers have reported pseudobinary phase diagrams for the DMPA/DMPC mixture at several pH values,[36] and they showed that, at pH 7 and T = 310 K, the 25% DMPA/DMPC mixture is in a fluid phase. At the same temperature but at pH 4, the mixture is in a mixed gel+fluid phase state and a macroscopic phase separation is observed.[36] Therefore, our results are in excellent agreement with the lipid phases experimentally observed.

The membrane thickness is a property which can be easily separated from its individual contributions. Therefore, in Figure 4 we show the separate contributions from DMPA and DMPC

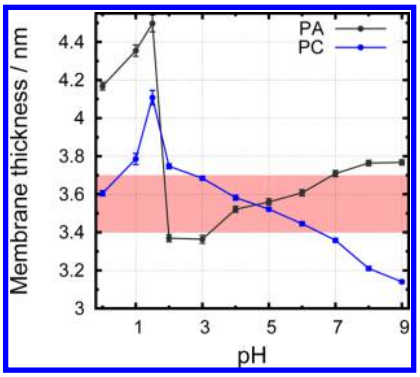

Figure 4. Average membrane thickness for PA and PC in the 25% DMPA/DMPC mixture as a function of pH. Typical experimental values range for liquid crystalline phase of DMPC is shown in red.[64]

to the membrane thickness at the different pH values. We observe that these two membrane constituents have rather different behaviors, in agreement with our previous study.[12] DMPC, as the major constituent of the bilayer is the lipid responsible for the phase transition, lowering its thickness with increasing pH. On the other hand, DMPA increases its thickness with pH, probably due to the need to solvate its more ionized phosphate groups and to interact more favorably with the available choline positive charges. The distributions of P atoms distances to the center of the bilayer (see Figure S2 in the Supporting Information) show a bell-shaped dispersion around the average values corresponding to Figure 4; the distributions tend to be slightly wider for PA, indicating an increased mobility along the membrane normal, probably due to oscillations in its ionization. At very low pH values (between pH 2.0 and 1.0), DMPA undergoes an apparent phase transition probably promoted by the protonated DMPC molecules (see also Figure S3 in the Supporting Information), which may explain why it was not observed in our previous MD study.[12] This ordering transition of DMPA (see below) can also explain the significant A_l variation observed between these pH values (Figure 3).

The deuterium order parameters allow us to follow the pH-induced phase transition focusing on the packing and ordering of the lipid tails. Once again, we were able to measure separately the contributions from DMPA and DMPC (Figure 5). From the pH dependence of the tails ordering, and quite similarly to the

DOI: 10.1021/acs.jctc.5b00956
J. Chem. Theory Comput. 2015, 11, 5973−5979

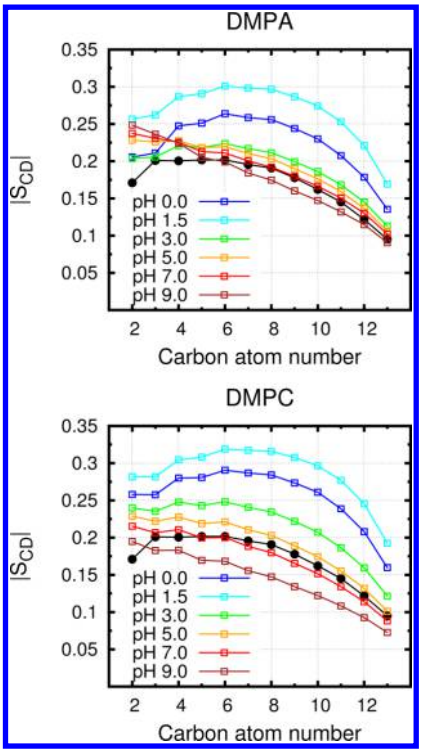

Figure 5. Deuterium order parameters for PA and PC in the 25% DMPA/DMPC mixture. An average contribution from both chains (*sn-1* and *sn-2*) is shown. Experimental curve for DMPC in the liquid crystalline phase is shown in black circles. These values were linearly interpolated to the desired temperature (310 K) from the three available temperature sets (303, 323, and 338 K).[65]

thickness parameter, PC seems to be the lipid undergoing the observed phase transition. PA remains relatively insensitive to pH, and only at very low pH its order parameter increases significantly, in line to what we have observed for the other structural parameters. These results are in agreement with the deuterium order parameters calculated from our previous fixed ionization MD study.[12] Interestingly, the tail ordering of both DMPA and DMPC at pH 7.0 is also in agreement with the experimental values for fluid pure DMPC,[65] which is another evidence that, at this pH value, our system represents closely the bilayer fluid phase.[36]

Lateral lipid diffusion is a measure of how fast lipids move in the *xy* plane. Figure 6 shows the diffusion constants at different pH values for both DMPA and DMPC. It seems that the different membrane thickness and lipid tail ordering between these two membrane constituents do not influence significantly their diffusion constants. There is a clear positive trend in both curves where upon increasing pH values, higher diffusion is seen. Only at very low pH values (<1.5), in the gel-like phase state, the diffusion constant values fall outside the typical experimental values range for fluid DMPC, as expected.

Several authors have presented experimental data and Monte Carlo simulations suggesting that in pseudobinary lipid systems there is clustering of like molecules and the formation of microdomains of different compositions.[36,70] In particular, the PA/PC lipid mixture has been proposed to undergo lipid immiscibility and even phase separation at pH 4.0.[36] These phenomena can have an important role in the biological function of PA-rich membranes.[6,7,9,10] The size of our 25% DMPA/DMPC lipid systems and the number of PA molecules do not allow the occurrence of microdomains or phase

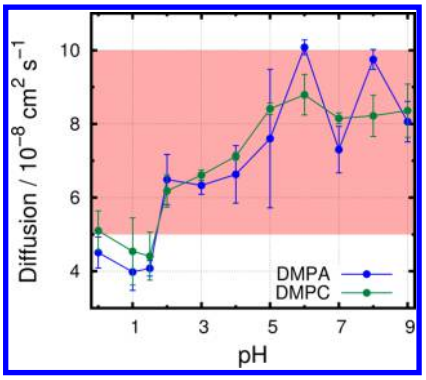

Figure 6. Lateral diffusion constants for PA and PC in the 25% DMPA/DMPC mixture as a function of pH. These values were obtained from the Einstein relation, measuring the slope of the mean square displacement over time. Typical experimental values range for liquid crystalline phase of DMPC is shown in red.[66−69]

separation. However, in our simulations, we can measure the DMPA aggregation tendency at the different pH values. Figure 7

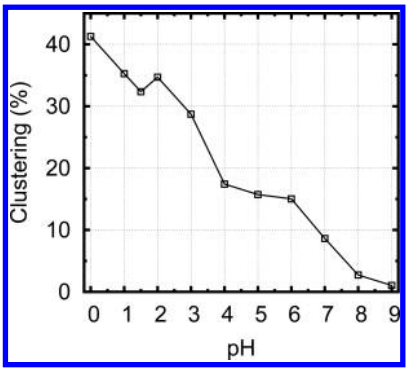

Figure 7. DMPA clustering tendency in the 25% DMPA/DMPC mixture measured by calculating the percentage of lipids involved in a cluster. A DMPA lipid is considered to be clustered if it is interacting, within a 5.5 Å cutoff, with at least another PA molecule. The choice of the cutoff value was based on the distance distribution between DMPA lipids in the same 25% DMPA/DMPC mixture (see the Supporting Information).

shows the fraction of lipids involved in PA—PA interactions at different pH values. Two DMPA molecules were considered to be interacting when their distance was below 5.5 Å (see Figure S4 in the Supporting Information). With decreasing pH, PA becomes less ionized and the hydrogen bonding tendency overcomes the electrostatic repulsion, allowing PA clustering. This PA aggregation was reversible in tens of nanoseconds and was observed in most simulations at low pH values. At pH 9.0, there is almost complete ionization and absence of hydrogen bond donors, which leads to complete disruption of PA aggregates. Figure 8 shows a membrane snapshot from one simulation at pH 3.0. Here, we observed a clear DMPA cluster where half of the available PA molecules aggregate (left panel of Figure 8). The cluster is stabilized by hydrogen bonding and decreased electrostatic repulsions. The ∼8 lipid molecules comprising the cluster show an average ionization of −0.24, while the remaining molecules are −0.89, for an average of −0.62 in all simulations at pH 3.0. The low ionization of the PA cluster can also help to rationalize its preferred deep inserted location (right panel of Figure 8). This internalization is favored by the lower need to solvate the cluster and by hydrogen

DOI: 10.1021/acs.jctc.5b00956
J. Chem. Theory Comput. 2015, 11, 5973−5979

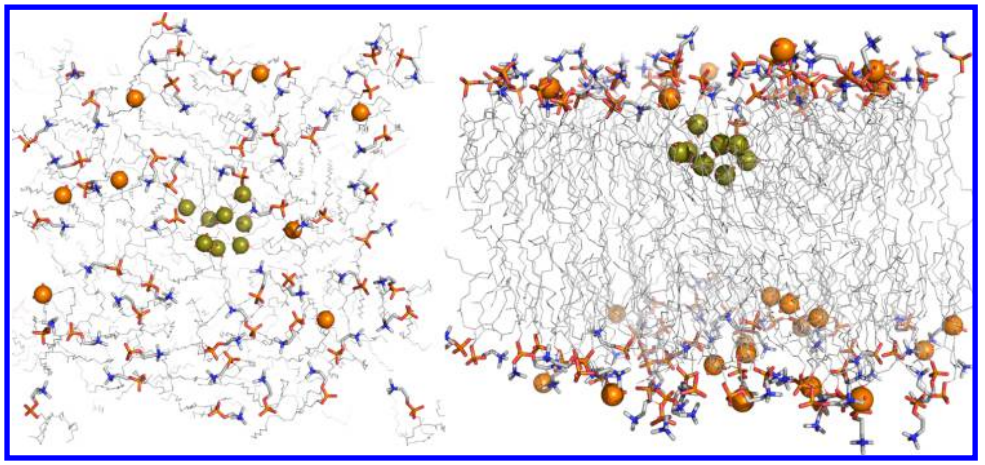

Figure 8. Graphic illustration of DMPA aggregation in the 25% DMPA/DMPC mixture at pH 3.0. The top view (left) helps identify the cluster, and in the side view (right), we can see its preferred location along the membrane normal. The P atoms from DMPA are shown in spheres with different colors, whether they belong to a cluster (olive) or not (orange). DMPC is shown only as sticks.

bonding of DMPA with the ester groups of DMPC, similar to what we have previously observed with a protonated DMPC molecule.[26] The Na^+ counterions do not seem to play a relevant role in this aggregation/insertion phenomena, unlike what has been observed for Ca^{2+} ions, whose internalization lead to a significant effect on the internal membrane electrostatic potential.[71]

4. CONCLUSIONS

In this work, we present a new extension of the CpHMD-L to study the pH effects on the DMPA/DMPC phospholipid mixture in a membrane model. As far as we know, this is the first CpHMD method used in continuous ("infinite") phospholipid bilayers with titration of all lipids in the membrane.

We performed a complete pH titration analysis and showed that, as expected, DMPA is more sensitive to pH changes and DMPC only contributes significantly to the total titration profile at pH values below 4.0, which is in agreement with our previous observations regarding this lipid.[26] Our results identified a pH region (pH 4.0−6.0) where there is coexistence of the three PA charge states (PA^0, PA^{-1}, and PA^{-2}) and a second one around pH 7.0, where the transition from PA^{-1} to PA^{-2} occurs. This transition at physiological pH indicates that any slight changes in the solution pH will have a major impact on the charge densities of these membranes, implicating PA as a key player in the regulation of many cellular events.[6,7,9,10]

Our study showed that the 25% DMPA/DMPC lipid bilayer system undergoes a pH-induced isothermal phase transition, in agreement to our previous work.[12] Also, at pH 4.0 and 7.0, the system is in the correct lipid phase, namely, gel/fluid mixture and completely fluid, respectively.[36] We presented several structural properties like A_l, membrane thickness, order parameter, and diffusion coefficient, which illustrate well the phase transition and the individual contributions from PA and PC. Very recently, a MM/MD study of DOPA in DPPC, where the authors just neutralized their systems with Na^+ ions, resulted in smaller A_l values for the double deprotonated PA^{-2} species compared with PA^{-1},[72] supporting the idea that a different approach, like the one presented here, is essential to correctly model these systems.

From our simulations, we also investigated the effects of pH in the aggregation tendency of DMPA. Indeed, when lowering the pH values, DMPA became more prone to hydrogen bonding and less prone to electrostatic repulsion, leading to an increase in clustering. Even though our simulation system is not large enough to observe immiscibility or phase separation phenomena,[36,70] we were able to identify and characterize small PA clusters.

This extension of the CpHMD-L method allows to simulate lipid bilayers with increased realism, since it allows the inclusion of anionic lipids titration in a phospholipid membrane model. It is now possible for the first time to simulate these systems with the correct treatment of ionization equilibrium, periodic boundary conditions, counterions, and ionic strength.

■ ASSOCIATED CONTENT

Supporting Information

The Supporting Information is available free of charge on the ACS Publications website at DOI: 10.1021/acs.jctc.5b00956.

Lipid bilayers composition, equilibration and production times, ions estimations for both MD and CpHMD simulations, titration curve with charge fluctuations test, distance histograms for DMPA (PDF)

■ AUTHOR INFORMATION

Corresponding Author

*Phone: 351-21-7500112. Fax: 351-21-7500088. E-mail: machuque@ciencias.ulisboa.pt.

Notes

The authors declare no competing financial interest.

■ ACKNOWLEDGMENTS

We thank Maria J. Calhorda and Sara R. R. Campos for fruitful discussions. We acknowledge financial support from Fundação para a Ciência e a Tecnologia through grant SFRH/BD/81017/2011 and projects PTDC/QUI-BIQ/113721/2009, PTDC/QEQ-COM/1623/2012, UID/MULTI/00612/2013, UID/MULTI/04046/2013, PEst-OE/EQB/LA0004/2011, and PTDC/QEQCOM/5904/2014.

■ REFERENCES

(1) Busa, W. B. *Annu. Rev. Physiol.* **1986**, *48*, 389−402.
(2) Kates, M.; Syz, J.-Y.; Gosser, D.; Haines, T. H. *Lipids* **1993**, *28*, 877−882.

DOI: 10.1021/acs.jctc.5b00956
J. Chem. Theory Comput. 2015, 11, 5973−5979

(3) Kurkdjian, A.; Guern, J. *Annu. Rev. Plant Physiol. Plant Mol. Biol.* **1989**, *40*, 271−303.
(4) Madshus, I. H. *Biochem. J.* **1988**, *250*, 1−8.
(5) Zhou, Y.; Raphael, R. *Biophys. J.* **2007**, *92*, 2451−2462.
(6) Loewen, C.; Gaspar, M.; Jesch, S.; Delon, C.; Ktistakis, N.; Henry, S.; Levine, T. *Science* **2004**, *304*, 1644−1647.
(7) Loew, S.; Kooijman, E. E.; May, S. *Chem. Phys. Lipids* **2013**, *169*, 9−18.
(8) Wang, X.; Devaiah, S. P.; Zhang, W.; R, W. *Prog. Lipid Res.* **2006**, *45*, 250−278.
(9) Young, B. P.; Shin, J. J. H.; Orij, R.; Chao, J. T.; Li, S. C.; Guan, X. L.; Khong, A.; Jan, E.; Wenk, M. R.; Prinz, W. A.; Smits, G. J.; Loewen, C. J. R. *Science* **2010**, *329*, 1085−1088.
(10) Shin, J. J. H.; Loewen, C. J. R. *BMC Biol.* **2011**, *9*, 85.
(11) Orij, R.; Brul, S.; Smits, G. J. *Biochim. Biophys. Acta, Gen. Subj.* **2011**, *1810*, 933−944.
(12) Vila-Viçosa, D.; Teixeira, V. H.; Santos, H. A. F.; Baptista, A. M.; Machuqueiro, M. *J. Chem. Theory Comput.* **2014**, *10*, 5483−5492.
(13) Baptista, A. M.; Teixeira, V. H.; Soares, C. M. *J. Chem. Phys.* **2002**, *117*, 4184−4200.
(14) Machuqueiro, M.; Baptista, A. M. *J. Phys. Chem. B* **2006**, *110*, 2927−2933.
(15) Machuqueiro, M.; Baptista, A. M. *Biophys. J.* **2007**, *92*, 1836−1845.
(16) Machuqueiro, M.; Baptista, A. M. *Proteins: Struct., Funct., Bioinf.* **2008**, *72*, 289−298.
(17) Machuqueiro, M.; Baptista, A. M. *J. Am. Chem. Soc.* **2009**, *131*, 12586−12594.
(18) Campos, S. R. R.; Machuqueiro, M.; Baptista, A. M. *J. Phys. Chem. B* **2010**, *114*, 12692−12700.
(19) Machuqueiro, M.; Baptista, A. M. *Proteins: Struct., Funct., Bioinf.* **2011**, *79*, 3437−3447.
(20) Vila-Viçosa, D.; Campos, S. R. R.; Baptista, A. M.; Machuqueiro, M. *J. Phys. Chem. B* **2012**, *116*, 8812−8821.
(21) Vila-ViÇosa, D.; Teixeira, V. H.; Santos, H. A. F.; Machuqueiro, M. *J. Phys. Chem. B* **2013**, *117*, 7507−7517.
(22) Henriques, J.; Costa, P. J.; Calhorda, M. J.; Machuqueiro, M. *J. Phys. Chem. B* **2013**, *117*, 70−82.
(23) Carvalheda, C. A.; Campos, S. R.; Machuqueiro, M.; Baptista, A. M. *J. Chem. Inf. Model.* **2013**, *53*, 2979−2989.
(24) Vila-ViÇosa, D.; Francesconi, O.; Machuqueiro, M. *Beilstein J. Org. Chem.* **2014**, *10*, 1513−1523.
(25) Vila-Viçosa, D.; Teixeira, V. H.; Baptista, A. M.; Machuqueiro, M. *J. Chem. Theory Comput.* **2015**, *11*, 2367−2376.
(26) Teixeira, V. H.; Vila-Viçosa, D.; Baptista, A. M.; Machuqueiro, M. *J. Chem. Theory Comput.* **2014**, *10*, 2176−2184.
(27) Torrie, G. M.; Valleau, J. P. *Chem. Phys. Lett.* **1979**, *65*, 343−346.
(28) Jönsson, B.; Wennerstroem, H.; Halle, B. *J. Phys. Chem.* **1980**, *84*, 2179−2185.
(29) Lakhdar-Ghazal, F.; Tichadou, J.-L.; Tocanne, J.-F. *Eur. J. Biochem.* **1983**, *134*, 531−537.
(30) Guldbrand, L.; Jönsson, B.; Wennerström, H.; Linse, P. *J. Chem. Phys.* **1984**, *80*, 2221−2228.
(31) Andelman, D. *Handb. Biol. Phys.* **1995**, *1*, 603−642.
(32) Peitzsch, R.; Eisenberg, M.; Sharp, K.; McLaughlin, S. *Biophys. J.* **1995**, *68*, 729−738.
(33) Smart, J.; McCammon, J. *J. Am. Chem. Soc.* **1996**, *118*, 2283−2284.
(34) Mengistu, D. H.; Kooijman, E. E.; May, S. *Biochim. Biophys. Acta, Biomembr.* **2011**, *1808*, 1985−1992.
(35) Israelachvili, J. N. *Intermolecular and surface forces, revised* 3rd ed.; Academic Press: 2011; pp 291−340.
(36) Garidel, P.; Johann, C.; Blume, A. *Biophys. J.* **1997**, *72*, 2196−2210.
(37) Oostenbrink, C.; Villa, A.; Mark, A. E.; van Gunsteren, W. F. *J. Comput. Chem.* **2004**, *25*, 1656−1676.
(38) Hermans, J.; Berendsen, H. J. C.; van Gunsteren, W. F.; Postma, J. P. M. *Biopolymers* **1984**, *23*, 1513−1518.
(39) Bussi, G.; Donadio, D.; Parrinello, M. *J. Chem. Phys.* **2007**, *126*, 014101.
(40) van der Ploeg, P.; Berendsen, H. J. C. *J. Chem. Phys.* **1982**, *76*, 3271−3275.
(41) Berendsen, H. J. C.; Postma, J. P. M.; van Gunsteren, W. F.; DiNola, A.; Haak, J. R. *J. Chem. Phys.* **1984**, *81*, 3684−3690.
(42) Hess, B. *J. Chem. Theory Comput.* **2008**, *4*, 116−122.
(43) Tironi, I. G.; Sperb, R.; Smith, P. E.; van Gunsteren, W. F. *J. Chem. Phys.* **1995**, *102*, 5451−5459.
(44) Smith, P.; van Gunsteren, W. *J. Chem. Phys.* **1994**, *100*, 3169−3174.
(45) Rocchia, W.; Sridharan, S.; Nicholls, A.; Alexov, E.; Chiabrera, A.; Honig, B. *J. Comput. Chem.* **2002**, *23*, 128−137.
(46) Li, L.; Li, C.; Sarkar, S.; Zhang, J.; Witham, S.; Zhang, Z.; Wang, L.; Smith, N.; Petukh, M.; Alexov, E. *BMC Biophys.* **2012**, *5*, 9.
(47) Schmid, N.; Eichenberger, A.; Choutko, A.; Riniker, S.; Winger, M.; Mark, A.; van Gunsteren, W. *Eur. Biophys. J.* **2011**, *40*, 843−856.
(48) Gilson, M.; Sharp, K.; Honig, B. *J. Comput. Chem.* **1988**, *9*, 327−335.
(49) Kumler, W.; Eiler, J. *J. Am. Chem. Soc.* **1943**, *65*, 2355−2361.
(50) Baptista, A. M.; Soares, C. M. *J. Phys. Chem. B* **2001**, *105*, 293−309.
(51) van der Spoel, D.; Lindahl, E.; Hess, B.; Groenhof, G.; Mark, A. E.; Berendsen, H. J. C. *J. Comput. Chem.* **2005**, *26*, 1701−1718.
(52) Hess, B.; Kutzner, C.; Van Der Spoel, D.; Lindahl, E. *J. Chem. Theory Comput.* **2008**, *4*, 435−447.
(53) Allen, M.; Tildesley, D. *Computer Simulation of Liquids*; Oxford University Press: USA, 1987.
(54) Nagle, J. F.; Wilkinson, D. A. *Biophys. J.* **1978**, *23*, 159−175.
(55) Janiak, M.; Small, D.; Shipley, G. *J. Biol. Chem.* **1979**, *254*, 6068−6078.
(56) Lis, L.; McAlister, M.; Fuller, N.; Rand, R.; Parsegian, V. *Biophys. J.* **1982**, *37*, 657.
(57) Lewis, B. A.; Engelman, D. M. *J. Mol. Biol.* **1983**, *166*, 211−217.
(58) Rand, R.; Parsegian, V. *Biochim. Biophys. Acta, Rev. Biomembr.* **1989**, *988*, 351−376.
(59) Koenig, B.; Strey, H.; Gawrisch, K. *Biophys. J.* **1997**, *73*, 1954−1966.
(60) Petrache, H.; Tristram-Nagle, S.; Nagle, J. *Chem. Phys. Lipids* **1998**, *95*, 83−94.
(61) Nagle, J. F.; Tristram-Nagle, S. *Curr. Opin. Struct. Biol.* **2000**, *10*, 474−480.
(62) Nagle, J.; Tristram-Nagle, S. *Biochim. Biophys. Acta, Rev. Biomembr.* **2000**, *1469*, 159−195.
(63) Kučerka, N.; Liu, Y.; Chu, N.; Petrache, H.; Tristram-Nagle, S.; Nagle, J. *Biophys. J.* **2005**, *88*, 2626−2637.
(64) Kučerka, N.; Nieh, M.-P.; Katsaras, J. *Biochim. Biophys. Acta, Biomembr.* **2011**, *1808*, 2761−2771.
(65) Petrache, H.; Dodd, S.; Brown, M. *Biophys. J.* **2000**, *79*, 3172.
(66) Rubenstein, J.; Smith, B. A.; McConnell, H. M. *Proc. Natl. Acad. Sci. U. S. A.* **1979**, *76*, 15−18.
(67) Alecio, M.; Golan, D.; Veatch, W.; Rando, R. *Proc. Natl. Acad. Sci. U. S. A.* **1982**, *79*, 5171−5174.
(68) Vaz, W.; Clegg, R.; Hallmann, D. *Biochemistry* **1985**, *24*, 781−786.
(69) Almeida, P.; Vaz, W. *Lateral diffusion in membranes*; Elsevier: 1995; Vol. *1*, pp 305−357.
(70) Hinderliter, A. K.; Huang, J.; Feigenson, G. W. *Biophys. J.* **1994**, *67*, 1906.
(71) Dias, R. P.; Li, L.; Soares, T. A.; Alexov, E. *J. Comput. Chem.* **2014**, *35*, 1418−1429.
(72) Kwolek, U.; Kulig, W.; Wydro, P.; Nowakowska, M.; Róg, T.; Kepczynski, M. *J. Phys. Chem. B* **2015**, *119*, 10042−10051.

DOI: 10.1021/acs.jctc.5b00956
J. Chem. Theory Comput. 2015, 11, 5973−5979